CHEMIJA
2026. Vol. 37. No. 3. P. 206–216

ISSN 0235-7216 eISSN 2424-4538
DOI: https://doi.org/10.6001/chemija.2026.37.3.3

Core planarisation suppresses delayed fluorescence in narrowband deep-blue tetraboron MR-TADF emitters

Giedrius Puidokas,

Lukas Deltuvytis,

Gediminas Kreiza,

Kristupas Bagdonas,

Karolis Kazlauskas*

Institute of Photonics and Nanotechnology,
Faculty of Physics,
Vilnius University,
3 Saulėtekio Avenue,
10257 Vilnius, Lithuania

Narrowband blue multiple-resonance thermally activated delayed fluorescence (MR-TADF) emitters are promising for high-colour-purity OLEDs, but structural modifications that preserve spectral purity can compromise delayed fluorescence. Here, two closely related tetraboron MR-TADF emitters, **BO-4B** and **c-BO-4B**, were designed to examine the effect of central-core planarisation on blue emission and triplet harvesting. The compounds were found to retain narrowband deep-blue fluorescence in dilute toluene, with emission maxima at 449 and 444 nm and full widths at half maximum of 14 and 19 nm, respectively. Quantum-chemical calculations indicate similar bright MR-type S_1 states but a larger singlet-triplet gap (ΔE_{ST}) for planarised **c-BO-4B**. Low-temperature fluorescence and phosphorescence measurements of PMMA films containing 1 wt% emitter show that core planarisation leaves the S_1 energy nearly unchanged while lowering T_1, thereby increasing ΔE_{ST} from 95 to 165 meV. Time-resolved fluorescence reveals an identical prompt fluorescence quantum yield of 33%, whereas the delayed fluorescence yield decreases from 45 to 3%. Within a simplified kinetic model, this corresponds to a two-order-of-magnitude decrease in a reverse intersystem crossing rate. These findings suggest that core planarisation preserves a narrow prompt emission but strongly suppresses a delayed fluorescence by unfavourably shifting triplet-state energetics.

Keywords: multiple resonance, thermally activated delayed fluorescence, tetraboron emitters, reverse intersystem crossing, narrowband blue emission

INTRODUCTION

Multiple-resonance thermally activated delayed fluorescence (MR-TADF) emitters are attractive organic luminescent materials because they combine narrowband emission with triplet harvesting through reverse intersystem crossing (RISC) [1–3]. Unlike conventional donor–acceptor TADF molecules, where long-range charge-transfer states often produce broad and environment-sensitive emission, MR emitters localise the excited-state redistribution within rigid heteroatom-doped polycyclic frameworks. This short-range charge-transfer character can provide a high oscillator strength, a small structural relaxation, and a high colour purity, which are especially valuable for blue organic light-emitting diode applications [2, 3]. Deep-blue narrowband MR-TADF emitters are particularly desirable because a high colour purity is required to approach the stringent blue-primary chromaticity defined by the ITU-R BT.2020 standard [4, 5].

Despite rapid progress, efficient RISC remains difficult to achieve and control in blue TADF emitters [6], including narrowband MR-TADF systems [7–9]. Although core rigidification is an attractive strategy for preserving a narrowband prompt emission by limiting excited-state relaxation, its effect on delayed fluorescence is less

* Corresponding author. Email: karolis.kazlauskas@ff.vu.lt

predictable. A small singlet–triplet energy splitting (ΔE_{ST}) is necessary for efficient TADF, but the RISC rate (k_{RISC}) also depends on the spin–orbit coupling, vibronic coupling, and the energetic accessibility of higher triplet states [7, 10, 11]. Thus, structural modifications that preserve spectral purity can still perturb triplet harvesting. This makes intentional core planarisation a useful test case for separating the requirements for a narrow prompt emission from those for an efficient delayed fluorescence.

Here, this issue is examined using two closely related boron/nitrogen-based MR emitters, **BO-4B** and **c-BO-4B**. The compounds share a similar emissive framework, but **c-BO-4B** contains an additional bridge in the central donor core, resulting in a more rigid and planarised structure. This molecular pair enables a direct comparison of how core planarisation affects the emissive singlet state, triplet-state energetics, and delayed fluorescence. The compounds were synthesised through a high-temperature boron-mediated cyclisation and characterised by steady-state and time-resolved photoluminescence spectroscopy, low-temperature emission measurements, single-crystal X-ray diffraction (XRD), and quantum-chemical calculations. The results show that core planarisation preserves a narrowband blue prompt emission but suppresses delayed fluorescence, consistent with increased ΔE_{ST} and a substantially reduced k_{RISC}.

EXPERIMENTAL

Methods and materials

Commercial chemicals were purchased from Sigma-Aldrich and used without further purification. The reactions were monitored by thin-layer chromatography on TLC silica gel 60 F254 aluminium sheets and by gas chromatography using an Agilent Technologies 6890N instrument. ^{1}H and ^{13}C NMR spectra were recorded on a Bruker Avance III (400 MHz and 101 MHz) spectrometer at ambient temperature. The chemical shifts (δ) are given in ppm relative to tetramethylsilane.

Absorption spectra of dilute toluene solutions (10^{-5} M) were measured using UV-vis-NIR spectrophotometer Lambda 950 (Perkin Elmer). PMMA films containing a 1 wt% emitter were prepared by spin-coating toluene solutions (80 mg/mL) on quartz substrates at 500 rpm, and annealed at 60°C for 10 min. Steady-state fluorescence (FL) spectra were recorded using a PMA-12 CCD spectrometer (Hamamatsu) under excitation at the corresponding absorption maxima with a xenon lamp coupled to a monochromator. Time-resolved FL spectra and decay transients were recorded using a nanosecond YAG:Nd^{3+} laser NT 242 equipped with an optical parametric oscillator (Ekspla, excitation wavelength 380 nm, pulse duration 5 ns, repetition rate 1 kHz) and a gated intensified CCD camera iStar DH340T (Andor) mounted on a spectrograph SR-303i (Shamrock). Low temperature measurements were performed in a closed-cycle helium cryostat 204 N (Cryo Industries). Toluene solutions were degassed by freeze-pump-thaw cycles prior to FL measurements. FL quantum yields (Φ_{FL}) were determined using an integrating sphere (Sphere Optics).

Single crystals of **c-BO-4B** suitable for XRD analysis were obtained by a slow evaporation of a tetrahydrofuran solution under ambient conditions. Data were collected at room temperature using an XtaLAB Synergy diffractometer (Rigaku) equipped with a HyPix-6000HE hybrid pixel detector and a PhotonJet Cu Kα X-ray source. Data collection, reduction and processing were performed using CrysAlisPro. The structure was solved by intrinsic phasing with SHELXT [12] and refined by full-matrix least-squares with SHELXL [13], as implemented in the Olex2 software environment [14]. The crystallographic information file (CIF) has been deposited with the Cambridge Crystallographic Data Centre (CCDC) under deposition number 2563431.

Geometry optimisations were performed using B3LYP/def2-SVP for the lowest-energy conformers identified by ORCA GOAT/GFN2-xTB [15, 16]. Vertical excited-state energies (S_1 and T_1), oscillator strengths, natural transition orbitals (NTOs), difference-density plots and spin-orbit coupling values were then calculated using time-dependent density functional theory (TD-DFT) at the B3LYP/def2-TZVP level in toluene. The calculated values were used for the qualitative comparison of two studied emitters.

1-Bromo-3,5-bis-phenoxy-benzene (1a)

1-Bromo-3,5-difluoro-benzene (29.0 g, 0.15 mol), phenol (42.0 g, 0.45 mol), potassium carbonate (83.0 g, 0.60 mol) and NMP (200 mL) were added to a 500 mL three-necked round bottom flask.

The reaction mixture was stirred and heated at 170°C overnight under argon atmosphere. The reaction mixture was added to water (1000 mL), extracted with hexane. The organic phase was washed with water, 5% NaOH solution and water again. The crude product was filtered through a pad of silica gel using hexane as an eluent, concentrated *in vacuo* and crystallised from methanol to give a compound (**1a**) as a white solid. Yield: 26.0 g (51%). ^{1}H NMR (400 MHz, $CDCl_3$) δ 7.40 (t, *J* = 8.0 Hz, 4H), 7.19 (t, *J* = 7.5 Hz, 2H), 7.07 (d, *J* = 7.6 Hz, 4H), 6.84 (d, *J* = 2.2 Hz, 2H), 6.63 (t, *J* = 2.2 Hz, 1H). ^{13}C NMR (101 MHz, $CDCl_3$) δ 159.45, 155.80, 130.01, 124.36, 123.04, 119.69, 115.77, 107.48, 77.36, 77.05, 76.73. MS (EI)*m*/*z* 340.1 [M^+].

1-Bromo-3,5-bis-(4-methyl-phenoxy)-benzene (1b)

1-Bromo-3,5-difluoro-benzene (11.6 g, 0.06 mol), *p*-cresol (19.6 g, 0.18 mol), potassium carbonate (37.3 g, 0.27 mol) and NMP (100 mL) were added to a 250 mL three-necked round bottom flask. The reaction mixture was stirred and heated at 170°C overnight under argon atmosphere. The reaction mixture was added to water (500 mL), extracted with hexane. The organic phase was washed with water, 5% NaOH solution and water again. The crude product was filtered through a pad of silica gel using hexane as an eluent, concentrated *in vacuo* and crystallised from an *i*-propanol/methanol mixture to give a compound (**1b**) as a white solid. Yield: 11.0 g (50%). ^{1}H NMR (400 MHz, $CDCl_3$) δ 7.08 (d, *J* = 8.2 Hz, 4H), 6.85 (d, *J* = 8.5 Hz, 4H), 6.67 (d, *J* = 2.2 Hz, 2H), 6.48 (t, *J* = 2.2 Hz, 1H), 2.26 (s, 6H). ^{13}C NMR (101 MHz, $CDCl_3$) δ 159.93, 153.36, 134.06, 130.49, 122.94, 119.79, 114.94, 106.71, 77.37, 77.06, 76.74, 20.81. MS (EI)*m*/*z* 368.1 [M^+].

3,5-di-bromo-*N*,*N*-diphenyl-amine (2a)

1,3,5-tri-bromo-benzene (4.0 g, 12.7 mmol), diphenylamine (2.0 g, 11.8 mmol), $Pd(OAc)_2$ (45 mg, 0.2 mmol), Xantphos (230 mg, 0.4 mmol), potassium *tert*-butoxide (2.6 g, 23.6 mmol) and dry toluene (50 mL) were added to a 100 mL round bottom flask. The reaction mixture was heated to reflux for 4 h under argon atmosphere. After cooling, the reaction mixture was filtered through a pad of silica gel using DCM as an eluent, concentrated *in vacuo*. The product was purified by flash chromatography using hexane/DCM (5:1) and crystallised from hexane to give a compound (**2a**) as a white solid. Yield: 2.6 g (54%). ^{1}H NMR (400 MHz, $CDCl_3$) δ 7.34 (t, *J* = 7.8 Hz, 4H), 7.22 (d, *J* = 1.8 Hz, 1H), 7.14 (dd, *J* = 11.0, 7.6 Hz, 6H), 7.09 (d, *J* = 1.7 Hz, 2H). ^{13}C NMR (101 MHz, $CDCl_3$) δ 150.30, 146.47, 129.71, 126.66, 125.36, 124.41, 123.21, 123.16, 77.38, 77.06, 76.74. MS (EI)*m*/*z* 403.0 [M^+].

N^1,N^3-dimesityl-N^5,N^5-diphenylbenzene-1,3,5-triamine (3a)

3,5-di-bromo-*N*,*N*-diphenyl-amine (**2a**) (2.2 g, 5.5 mmol), 2,4,6-trimethylaniline (2.2 g, 16.5 mmol), $Pd(OAc)_2$ (23 mg, 0.1 mmol), Xantphos (100 mg, 0.2 mmol), sodium *tert*-butoxide (1.9 g, 20.0 mmol) and dry toluene (50 mL) were added to a 100 mL round bottom flask. The reaction mixture was heated at 90°C for 5 h under argon atmosphere. After cooling, the reaction mixture was filtered through a pad of silica gel using DCM as an eluent, concentrated *in vacuo*. The product was crystallised from hexane to give a compound (**3a**) as a yellow solid. Yield: 2.0 g (71%). ^{1}H NMR (400 MHz, $CDCl_3$) δ 7.26–7.16 (m, 4H), 7.08 (dd, *J* = 7.3, 1.5 Hz, 4H), 6.96 (td, *J* = 7.2, 1.2 Hz, 2H), 6.87 (s, 4H), 5.65 (d, *J* = 2.0 Hz, 2H), 5.42 (t, *J* = 2.0 Hz, 1H), 4.87 (s, 2H), 2.28 (s, 6H), 2.17 (s, 12H). ^{13}C NMR (101 MHz, $CDCl_3$) δ 149.34, 148.43, 147.87, 135.76, 135.62, 134.93, 129.01, 128.76, 123.76, 121.88, 101.27, 94.51, 77.36, 77.04, 76.72, 20.85, 18.30. MS (EI)*m*/*z* 511.4 [M^+].

9-(3,5-dibromophenyl)-9*H*-carbazole (2b)

1,3,5-tri-bromo-benzene (23.6 g, 75.0 mmol), 9*H*-carbazole (8.4 g, 50.0 mmol), potassium carbonate (8.3 g, 60.0 mmol), copper (I) iodide (0.48 g, 2.5 mmol), 1,10-phenanthroline hydrochloride (0.54 g, 2.5 mmol) and 100 mL DMF were added to a 250 mL three-necked round bottom flask. The reaction mixture was stirred and heated to reflux overnight under argon atmosphere. The reaction mixture was added to water (500 mL), extracted with DCM. The organic phase was concentrated *in vacuo*. The crude product was purified by column chromatography on a silica gel column with hexane as an eluent to obtain a compound (**2b**) as a white solid. Yield: 6.0 g (29%). ^{1}H NMR (400 MHz, $CDCl_3$) δ 8.13(d, *J* = 7.8 Hz, 2H), 7.79 (s, 1H), 7.72 (d, *J* = 1.7 Hz, 2H), 7.44–7.40 (m, 4H),7.31(t,

J = 8.0, 2H). ^{13}C NMR(101 MHz, $CDCl_3$) δ 140.28, 140.05, 132.96, 128.86, 126.30, 123.65, 120.70, 120.37, 109.55. MS (EI)*m*/*z* 401.0 [M^+].

5-(9*H*-carbazol-9-yl)-*N*^{1},*N*^{3}-dimesitylbenzene-1,3-diamine (3b)

9-(3,5-dibromophenyl)-9*H*-carbazole (**2b**) (1.6 g, 4.0 mmol), 2,4,6-trimethylaniline (1.2 g, 8.8 mmol), $Pd(OAc)_2$ (18 mg, 0.08 mmol), Xantphos (92 mg, 0.16 mmol), sodium *tert*-butoxide (1.3 g, 13.2 mmol) and dry toluene (30 mL) were added to a 100 mL round bottom flask. The reaction mixture was heated at 90°C for 5 h under argon atmosphere. After cooling, the reaction mixture was filtered through a pad of silica gel using DCM as an eluent, concentrated *in vacuo*. The product was crystallised from hexane to give a compound (**3b**) as an off-white solid. Yield: 1.2 g (58%). ^{1}H NMR (400 MHz, $CDCl_3$) δ 8.10 (d, *J* = 7.7 Hz, 2H), 7.46 (d, *J* = 8.2 Hz, 2H), 7.40 (ddd, *J* = 8.3, 7.0, 1.2 Hz, 2H), 7.27–7.22 (m, 2H), 6.92 (s, 4H), 6.00 (d, *J* = 2.1 Hz, 2H), 5.85 (t, *J* = 2.1 Hz, 1H), 5.12 (s, 2H), 2.29 (s, 12H), 2.28 (s, 6H). ^{13}C NMR (101 MHz, $CDCl_3$) δ 149.11, 140.88, 139.45, 136.12, 135.68, 135.31, 131.61, 129.24, 125.59, 123.01, 120.06, 119.31, 110.32, 102.09, 97.47, 77.38, 77.07, 76.75, 20.91, 18.37. MS (EI)*m*/*z* 509.3 [M^+].

Intermediate 1 (4a)

N^1,*N*^{3}-dimesityl-*N*^{5},*N*^{5}-diphenylbenzene-1,3,5-triamine (**3a**) (0.30 g, 0.64 mmol), 1-bromo-3,5-bis-phenoxy-benzene (**1a**) (0.66 g, 1.92 mmol), $Pd_2(dba)_3$ (12 mg, 0.01 mmol), *t*-$Bu_3P{\cdot}HBF_4$ (12 mg, 0.04 mmol), sodium *tert*-butoxide (0.40 g, 4.0 mmol) and dry toluene (30 mL) were added to a 100 mL round bottom flask. The reaction mixture was heated to reflux overnight under argon atmosphere. After cooling, the reaction mixture was filtered through a pad of silica gel using DCM as an eluent, concentrated *in vacuo*. The crude product was purified by column chromatography on a silica gel column with hexane/DCM (5:1) as an eluent to obtain a compound (**4a**) as a white solid. Yield: 0.39 g (60%). ^{1}H NMR (400 MHz, $CDCl_3$) δ 7.33–7.22 (m, 8H), 7.17 (t, *J* = 7.7 Hz, 4H), 7.10–6.99 (m, 8H), 6.92 (d, *J* = 7.7 Hz, 8H), 6.87 (t, *J* = 7.3 Hz, 2H), 6.77 (s, 4H), 6.49 (d, *J* = 2.0 Hz, 2H), 6.32 (d, *J* = 2.1 Hz, 4H), 5.97 (t, *J* = 2.1 Hz, 2H), 5.92 (t, *J* = 2.1 Hz, 1H), 2.26 (s, 6H), 1.91 (s, 12H). ^{13}C NMR (101 MHz, $CDCl_3$) δ 158.33, 156.91, 148.56, 148.34, 147.27, 146.21, 139.26, 136.88, 136.71, 129.66, 129.59, 129.07, 123.81, 123.00, 122.50, 118.39, 110.31, 108.47, 104.48, 101.06, 77.37, 77.05, 76.73, 20.96, 18.17.

Intermediate 2 (4b)

5-(9*H*-carbazol-9-yl)-*N*^{1},*N*^{3}-dimesitylbenzene-1,3-diamine (**3b**) (0.30 g, 0.64 mmol), 1-bromo-3,5-bis-(4-methyl-phenoxy)-benzene (**1b**) (0.74 g, 1.92 mmol), $Pd_2(dba)_3$ (12 mg, 0.01 mmol), *t*-$Bu_3P{\cdot}HBF_4$ (12 mg, 0.04 mmol), sodium *tert*-butoxide (0.40 g, 4.0 mmol) and dry toluene (30 mL) were added to a 100 mL round bottom flask. The reaction mixture was heated to reflux overnight under argon atmosphere. After cooling, the reaction mixture was filtered through a pad of silica gel using DCM as an eluent, concentrated *in vacuo*. The crude product was purified by column chromatography on a silica gel column with hexane/DCM (5:1) as an eluent to obtain a compound (**4b**) as a white solid. Yield: 0.51 g (76%). ^{1}H NMR (400 MHz, $CDCl_3$) δ 8.12 (d, *J* = 7.6 Hz, 2H), 7.36–7.19 (m, 6H), 7.00 (d, *J* = 8.2 Hz, 8H), 6.84 (d, *J* = 5.0 Hz, 8H), 6.81 (s, 4H), 6.77 (d, *J* = 2.0 Hz, 2H), 6.59 (d, *J* = 2.2 Hz, 1H), 6.46 (d, *J* = 2.1 Hz, 4H), 6.04 (t, *J* = 2.1 Hz, 2H), 2.28 (s, 6H), 2.27 (s, 12H), 2.01 (s, 12H). ^{13}C NMR (101 MHz, $CDCl_3$) δ 159.05, 154.39, 147.75, 147.35, 140.22, 139.30, 138.73, 137.06, 136.94, 132.69, 130.09, 129.93, 125.89, 123.30, 120.13, 119.78, 118.51, 110.89, 110.06, 104.80, 101.29, 77.36, 77.04, 76.72, 20.99, 20.63, 18.30.

BO-4B

Intermediate 1 (**4a**) (0.31 g, 0.30 mmol) was dissolved in extra dry 1,2-dichlorobenzene (5 mL) and added to a 120 mL pressure flask. Boron tribromide (3.0 g, 1.1 mL, 12.0 mmol) was added to the reaction mixture under argon atmosphere. The flask was sealed and heated at 200°C for 48 h. After cooling in an ice bath, methanol was slowly added to quench the reaction. The mixture was concentrated *in vacuo*. The crude product was dissolved in 30 mL toluene and 2 mL acetic acid was added. This mixture was refluxed for 2 h, concentrated *in vacuo*. The crude product was purified by column chromatography on a silica gel column with hexane/DCM (10:1) as an eluent and crystallised from a hexane/DCM mixture to obtain a compound (**BO-4B**) as a yellow solid. Yield: 0.08 g (26%). ^{1}H NMR (400 MHz, $CDCl_3$) δ 8.98 (dd, *J* = 7.7,

1.7 Hz, 2H), 8.79 (dd, *J* = 23.1, 7.6 Hz, 4H), 8.49 (d, *J* = 8.5 Hz, 2H), 7.80 (dd, *J* = 3.8, 1.6 Hz, 2H), 7.71–7.62 (m, 4H), 7.54–7.48 (m, 2H), 7.45 (dt, *J* = 9.8, 4.5 Hz, 4H), 7.40 (d, *J* = 7.4 Hz, 2H), 7.22 (dd, *J* = 7.9, 6.0 Hz, 2H), 7.07 (s, 2H), 6.98 (s, 2H), 6.62 (s, 2H), 5.47 (s, 1H), 2.53 (s, 6H), 1.83 (s, 6H), 1.73 (s, 6H).

c-BO-4B

Intermediate 2 (**4b**) (0.8 g, 0.72 mmol) was dissolved in extra dry 1,2-dichlorobenzene (5 mL) and added to a 120 mL pressure flask. Boron tribromide (7.2 g, 2.7 mL, 28.8 mmol) was added to the reaction mixture under argon atmosphere. The flask was sealed and heated at 200°C for 48 h. After cooling in an ice bath, methanol was slowly added to quench the reaction. The mixture was concentrated *in vacuo*. The crude product was dissolved in 30 mL toluene and 2 mL acetic acid was added. This mixture was refluxed for 2 h, concentrated *in vacuo*. The crude product was filtered through a pad of silica gel using hot toluene as an eluent, concentrated *in vacuo*. The product was crystallised from toluene and washed with acetone to give a compound (**c-BO-4B**) as a green solid. Yield: 0.32 g (40%). ^{1}H NMR (400 MHz, $CDCl_3$) δ 9.51 (d, *J* = 7.9 Hz, 2H), 8.65 (d, *J* = 7.4 Hz, 2H), 8.63–8.52 (m, 4H), 7.90 (d, *J* = 7.9 Hz, 2H), 7.69 (d, *J* = 8.8 Hz, 2H), 7.50 (d, *J* = 8.2 Hz, 2H), 7.22 (d, *J* = 7.8 ***Hz,*** 4H), 7.04 (s, 4H), 6.62 (s, 2H), 5.56 (s, 1H), 2.59 (s, 6H), 1.83 (s, 12H), 1.58 (s, 12H).

RESULTS AND DISCUSSION

Synthesis

The molecular structures of **BO-4B** and **c-BO-4B** and their synthetic routes are presented in Scheme 1. The synthesis started with bis(aryloxy)-bromobenzene precursors prepared by thermal nucleophilic aromatic substitution (S_NAr), while the amine and carbazole building blocks were obtained by Buchwald–Hartwig or Cu-catalysed Ullmann coupling reactions. Subsequent Pd-catalysed C–N coupling afforded intermediates 4a and 4b, which were converted into **BO-4B** and **c-BO-4B** by BBr_3-mediated one-pot tetra-borylation/cyclisation at 200°C.

This late-stage borylation strategy differs from reported routes to related tetraboron MR emitters, such as tBO-4B [17], 4M-BOB4 and 4F-BOB4 [18], in which DOBNA-type fragments are preinstalled prior to the final framework extension. In the present route, all boron atoms are introduced during the final cyclisation step, affording **BO-4B** and **c-BO-4B** with improved isolated yields of 26 and 40%, respectively.

The structures of **BO-4B** and **c-BO-4B** were confirmed by ^{1}H NMR spectroscopy, and the structure of **c-BO-4B** was further confirmed by single-crystal XRD. Acquisition of ^{13}C NMR spectra was not feasible due to the limited solubility of the compounds.

X-ray diffraction

The molecular structure of **c-BO-4B** was confirmed by single-crystal XRD analysis (Fig. 1). The compound crystallises in the triclinic crystal system with the centrosymmetric space group $P\bar{1}$. The unit cell parameters are *a* = 18.6748(2) Å, *b* = 19.7507(2) Å, *c* = 22.0285(2) Å, α = 113.6710(10)°, β = 98.6290(10)° and γ = 100.8530(10)°, corresponding to a unit-cell volume of 7074.64(14) Å^3 with *Z* = 2. The crystallographic structure verifies the fused and planarised central donor core of **c-BO-4B**.

Quantum-chemical analysis

The quantum-chemical calculations clarify the structural effect of core cyclisation. In **BO-4B**, the central core has a phenyl-phenyl dihedral angle of 58.4°, whereas the additional intramolecular bridge in **c-BO-4B** locks this core into a planar arrangement. This provides a direct basis for evaluating how planarisation of the MR framework affects the singlet and triplet excited states.

The TD-DFT calculations (Table 1) reproduce the main qualitative trends observed experimentally. In particular, they predict a higher S_1 energy for **c-BO-4B** than for **BO-4B** in both the S_0 and S_1 geometries, consistent with the blue-shifted absorption and fluorescence observed in a toluene solution. A larger ΔE_{ST} is also predicted for **c-BO-4B** at both geometries. Although the calculated absolute gaps are larger than the experimental values, the predicted increase in ΔE_{ST} upon core cyclisation is consistent with the experiment.

The S_1 NTOs in Fig. 2 show complementary hole and particle distributions over alternating regions of the same rigid π-framework, which is typical of a multiple-resonance excitation rather than a conventional long-range donor–acceptor charge-transfer state. The nearly identical $S_0 \rightarrow S_1$

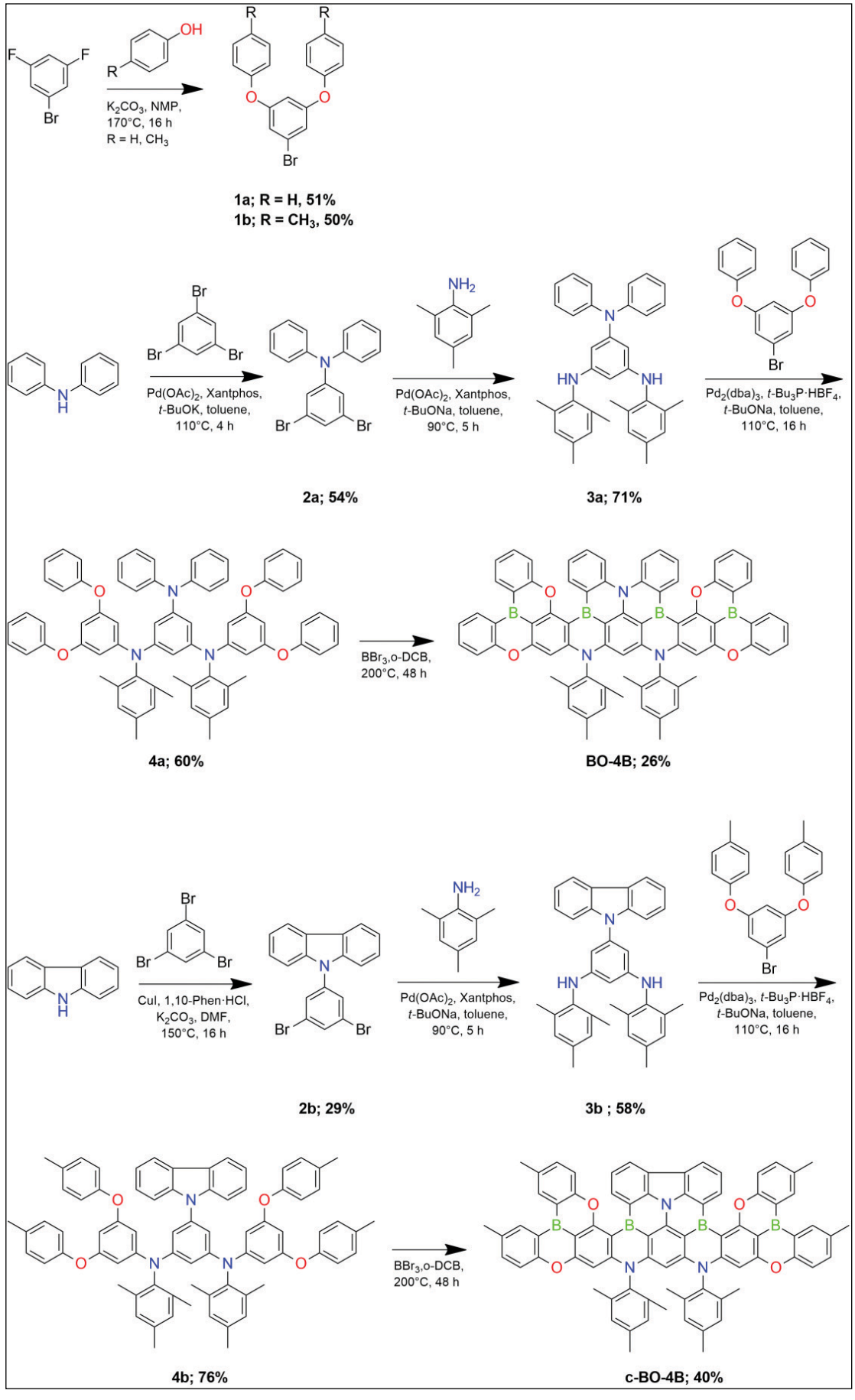

Scheme 1. Synthetic route to tetraboron MR emitters **BO-4B** and **c-BO-4B**

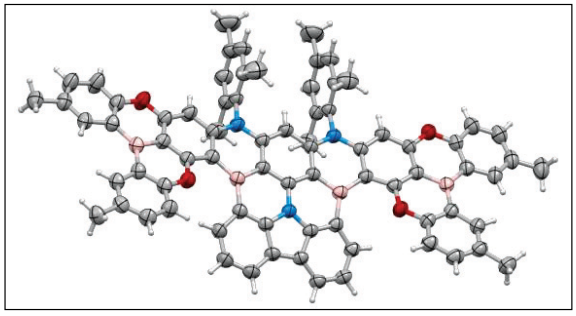

Fig. 1. Molecular structure of **c-BO-4B** determined by single-crystal XRD. Thermal ellipsoids are shown at the 50% probability level, and hydrogen atoms are represented as small spheres for clarity

oscillator strengths of **BO-4B** and **c-BO-4B** further indicate that core planarisation has a little effect on the calculated strength of the lowest singlet transition.

The difference-density plots indicate a stronger effect of planarisation on the triplet state than on the emissive singlet state. For **BO-4B**, the S_1 and T_1 difference densities show broadly similar redistribution patterns, consistent with a very weak direct S_1–T_1 spin–orbit coupling (SOC = 0.03 cm^{-1}). For **c-BO-4B**, the T_1 redistribution differs more clearly from S_1, and the calculated SOC increases by about

Table 1. **TD-DFT-calculated first singlet and triplet excitation energies, singlet–triplet energy gaps, and oscillator strengths of the studied compounds at S_0- and S_1-optimised geometries**

	Geometry	S_1, eV	T_1, eV	ΔE_{ST}, meV	f ($S_0 \rightarrow S_1$)
BO-4B	S_0	2.781	2.581	200	0.728
	S_1	2.724	2.529	195	
c-BO-4B	S_0	2.861	2.586	275	0.726
	S_1	2.810	2.560	250	

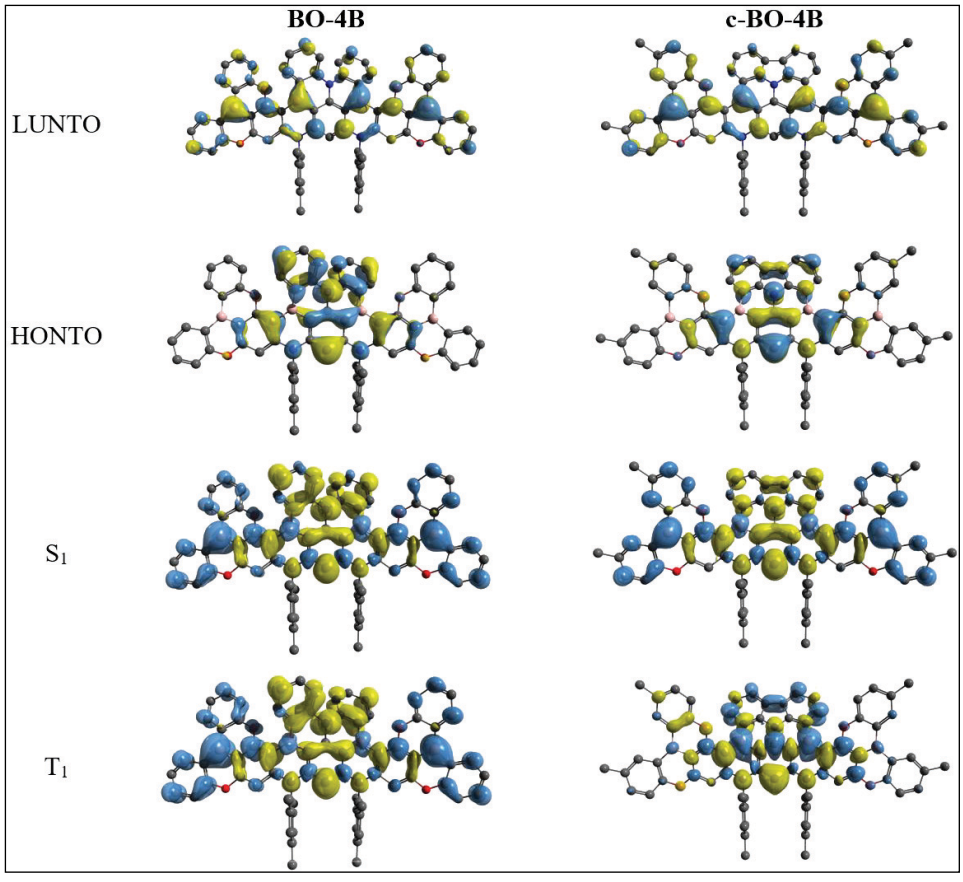

Fig. 2. Calculated S_1 natural transition orbitals and TD-DFT difference-density plots for **BO-4B** and **c-BO-4B**. Hole and particle NTOs are shown with an isovalue of 0.025. S_1 and T_1 difference-density plots are shown with an isovalue of 0.0005, where blue and yellow regions indicate increased and decreased electron density upon excitation, respectively

one order of magnitude (SOC = 0.32 cm^{-1}). Thus, the calculations suggest that core planarisation preserves a bright MR-type S_1 transition but modifies the triplet-state character and increases ΔE_{ST}.

Photophysical properties

The calculated trends are reflected in the room-temperature optical spectra (Fig. 3). In the dilute toluene solution, **c-BO-4B** shows a blue-shifted low-energy absorption maximum at 432 nm, compared with 441 nm for **BO-4B**. Its fluorescence maximum is likewise blue-shifted from 449 to 444 nm. Thus, despite the additional central-core connection, core planarisation does not red-shift the emissive singlet state. **c-BO-4B** shows a slightly larger Stokes shift, increasing from approximately 50 meV for **BO-4B** to 80 meV, and a broader emission band, with the FWHM increasing from 14 to 19 nm. Nevertheless, both compounds retain a narrowband deep-blue emission.

The S_1 and T_1 energies (Table 2) were estimated from the low-temperature fluorescence and phosphorescence spectra of 1 wt% PMMA films. In this matrix, the two compounds have the same estimated S_1 energy of 2.74 eV, whereas T_1 is lower for **c-BO-4B** (2.58 eV) compared to **BO-4B** (2.65 eV). Consequently, ΔE_{ST} increases from 95 meV for **BO-4B** to 165 meV for **c-BO-4B**. The larger ΔE_{ST} of **c-BO-4B** therefore arises mainly from the stabilisation of T_1, while S_1 remains essentially unchanged.

The time-resolved FL measurements (Figs. 4 and 5) reveal clear differences between the two emitters. **c-BO-4B** has longer prompt and delayed FL lifetimes, with τ_{PF} = 4.5 ns and τ_{DF} = 8 µs, compared with 2.5 ns and 1 µs for **BO-4B**. Φ_{PL} was separated into prompt (Φ_{PF}) and delayed (Φ_{DF}) contributions based on the relative integrated areas of the fitted transient components [19]. Both compounds have the same Φ_{PF} = 33%, whereas Φ_{DF} decreases from 45% for **BO-4B** to only 3% for **c-BO-4B**. The lower

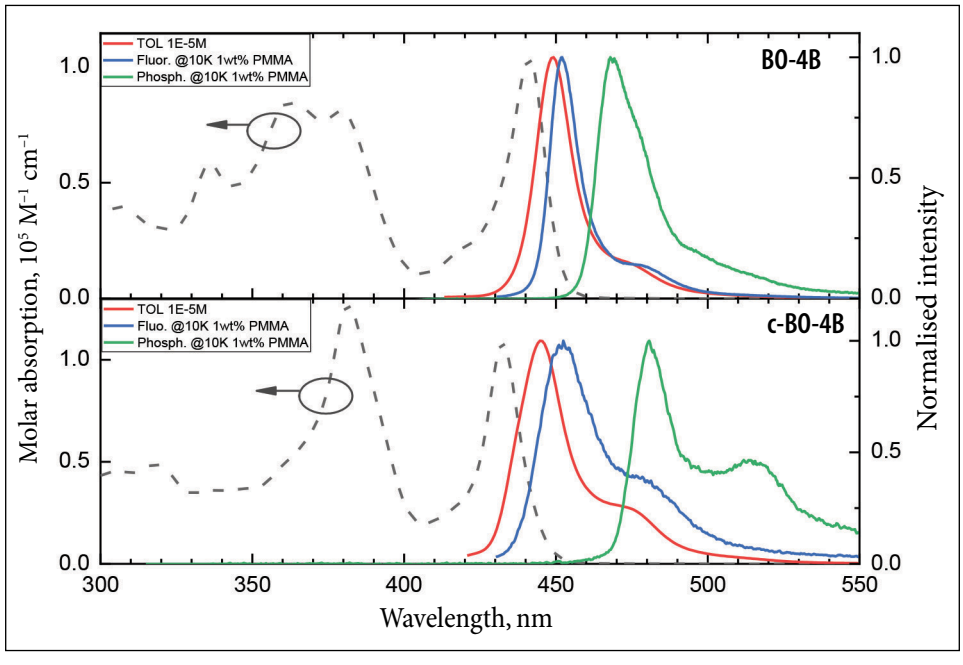

Fig. 3. Absorption (dashed line) and normalised fluorescence spectra (red line) of dilute toluene solutions of **BO-4B** and **c-BO-4B** at room temperature, together with normalised fluorescence (blue line) and phosphorescence (green line) spectra of 1 wt% doped PMMA films recorded at 10 K

Table 2. **Photophysical properties of BO-4B and c-BO-4B in the dilute toluene solution at room temperature and in 1 wt% PMMA films at 10 K**

	10^{-5} M TOL											1 wt% PMMA		
	λ_{PL}, nm	FWHM, nm	Φ_{PL}, %	Φ_{PF}, %	Φ_{DF}, %	τ_{PF}, ns	τ_{DF}, µs	k_r, 10^6 s^{-1}	k_{ISC}, 10^6 s^{-1}	k_{RISC}, 10^6 s^{-1}	k_{nr}, T, 10^6 s^{-1}	S_1, eV	T_1, eV	ΔE_{ST}, meV
BO-4B	449	14	78	33	45	2.5	1	130	267	2	0.31	2.74	2.65	95
c-BO-4B	444	19	36	33	3	4.5	8	72	146	0.02	0.12	2.74	2.58	165

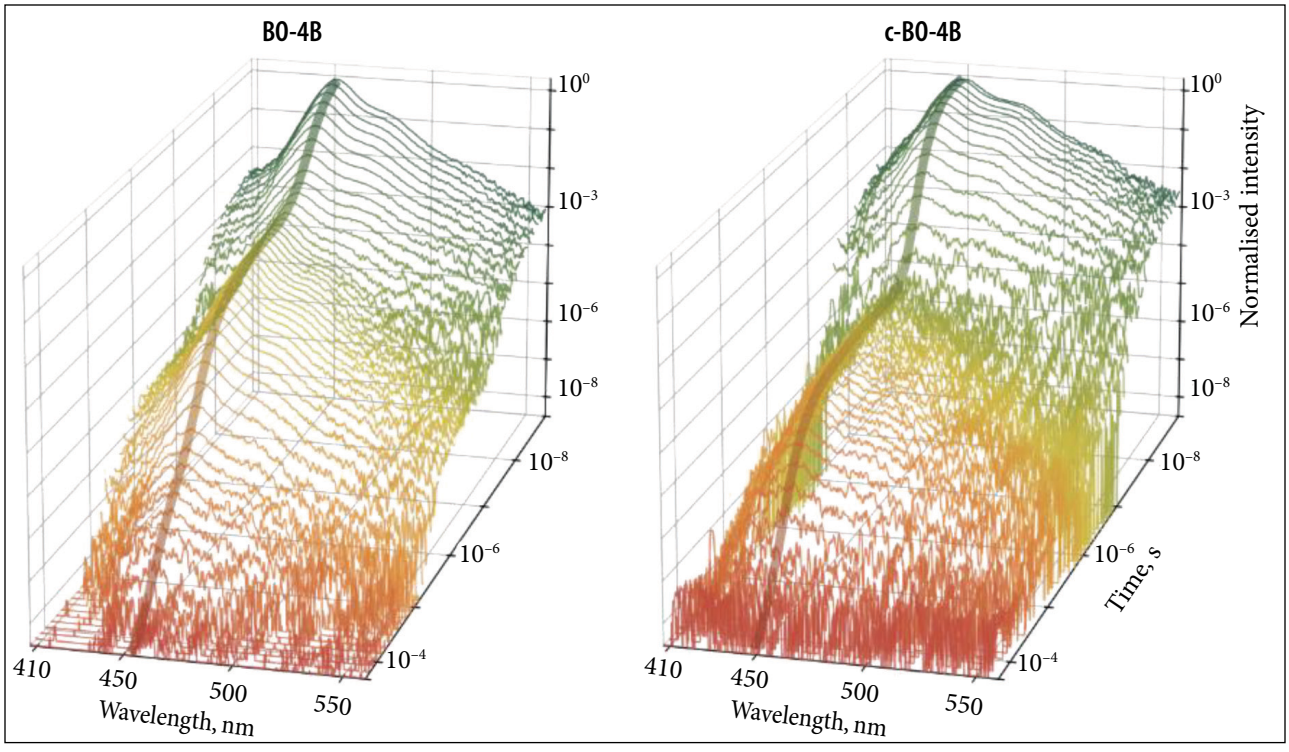

Fig. 4. Time-resolved FL spectra of dilute toluene solutions of **BO-4B** and **c-BO-4B** showing the temporal evolution of prompt and delayed emission components. Guide lines mark the emission maxima

Φ_{PL} of **c-BO-4B** therefore results mainly from its strongly suppressed delayed fluorescence.

The rate constants in Table 2 were extracted using a simplified three-state kinetic model, assuming that the dominant non-radiative loss occurs from the triplet state [19, 20]. The radiative decay rate (k_r) and the intersystem crossing rate (k_{ISC}) are approximately twice as high for **BO-4B** than for **c-BO-4B**. The largest difference, however, is observed for the k_{RISC}, which decreases two orders of magnitude from 2×10^6 s^{-1} for **BO-4B** to 0.02×10^6 s^{-1} for **c-BO-4B**.

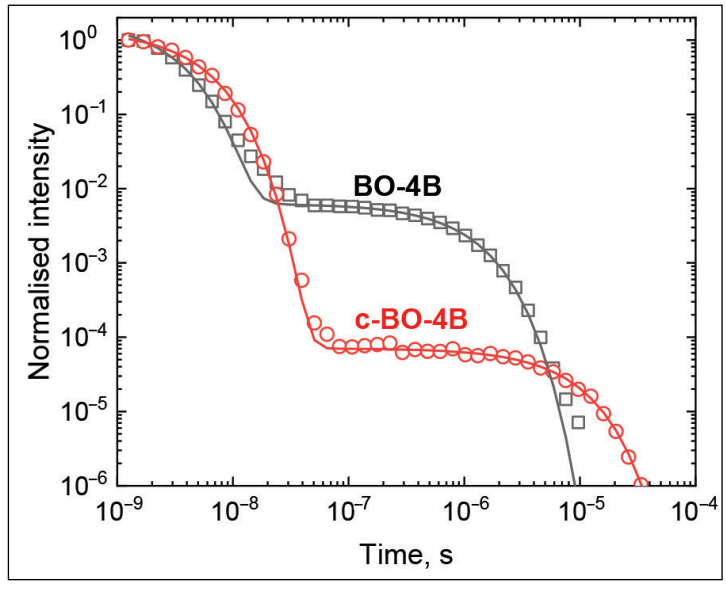

Fig. 5. Fluorescence decay transients of dilute toluene solutions of **BO-4B** and **c-BO-4B** (points). Lines show double-exponential fits used to extract prompt and delayed lifetimes for the kinetic analysis

For **BO-4B**, k_{RISC} exceeds the non-radiative triplet decay rate ($k_{nr,\,T}$), enabling an efficient triplet upconversion and a strong delayed FL contribution. In contrast, for **c-BO-4B**, k_{RISC} becomes smaller than the $k_{nr,\,T}$, consistent with enhanced triplet losses, which result in much smaller Φ_{DF} and Φ_{PL} of **c-BO-4B**.

The larger ΔE_{ST} of **c-BO-4B** is consistent with slower RISC. Under a simple Boltzmann-type dependence with comparable prefactors, the 70 meV increase in ΔE_{ST} would predict k_{RISC} ratio of only ca. 15:

$$\frac{k_{RISC}^{BO-4B}}{k_{RISC}^{c-BO-4B}} = \frac{e^{-\Delta E_{ST}^{BO-4B}/k_B T}}{e^{-\Delta E_{ST}^{c-BO-4B}/k_B T}} = e^{(165-95)/25.7} \approx 15.$$

The experimentally obtained ratio is significantly larger, approaching two orders of magnitude, likely indicating an additional contribution from changes in the triplet-state character, vibronic coupling, and/or the involvement of higher-lying triplet states [7, 10, 11]. Thus, the paired comparison unveils a clear decoupling of the prompt and delayed emission channels, where central-core planarisation preserves narrowband blue FL while making triplet harvesting via RISC substantially less efficient.

CONCLUSIONS

Central-core planarisation was found to decouple prompt and delayed emission in tetraboron MR-TADF emitters. It preserved the narrowband deep-blue FL but strongly suppressed the delayed FL. This effect was established by comparing a structurally matched pair of emitters, **BO-4B** and **c-BO-4B**, synthesised through a late-stage BBr_3-mediated tetra-borylation/cyclisation strategy. Core planarisation in **c-BO-4B** is consistent with the expected benefit of a more rigid MR framework in limiting excited-state structural relaxation. Both compounds retain the same prompt fluorescence quantum yield of 33%, and TD-DFT calculations indicate similar bright MR-type S_1 states with nearly identical oscillator strengths.

The main effect of core planarisation is instead observed in the triplet-related properties. **c-BO-4B** shows a lower T_1 and a larger ΔE_{ST}, increasing from 95 to 165 meV, together with a modified calculated T_1 difference-density pattern. The time-resolved FL analysis reveals that the decrease in delayed FL yield from 45 to 3% is accompanied by a two-order-of-magnitude reduction in k_{RISC}. These results demonstrate that sustaining a bright and narrow MR-type singlet state is not sufficient to maintain an efficient delayed FL. In fact, central-core planarisation preserves a prompt blue emission but compromises triplet harvesting by shifting the triplet energetics and slowing RISC relative to triplet loss. Thus, core rigidification and efficient triplet harvesting must be optimised independently in the design of narrowband MR-TADF emitters.

ACKNOWLEDGEMENTS

Authors acknowledge the 'Universities' Excellence Initiative' programme by the Ministry of Education, Science and Sports of the Republic of Lithuania under the agreement with the Research Council of Lithuania (Project No. S-A-UEI-236).

Received 26 June 2026
Accepted 2 July 2026

References

1. H. Uoyama, K. Goushi, K. Shizu, H. Nomura, C. Adachi, *Nature*, **492**, 234 (2012).
2. T. Hatakeyama, K. Shiren, K. Nakajima, et al., *Adv. Mater.*, **28**, 2777 (2016).
3. M. Mamada, M. Hayakawa, J. Ochi, T. Hatakeyama, *Chem. Soc. Rev.*, **53**, 1624 (2024).
4. J. Jin, Z. He, D. Liu, et al., *Chem. Sci.*, **15**, 18135 (2024).
5. Z. Xue, Z. Xiao, Y. Zou, et al., *Chem. Sci.*, **16**, 3655 (2025).
6. G. Kreiza, T. Javorskis, E. Orentas, K. Kazlauskas, *Adv. Optical Mater.*, **12**, 2400024 (2024).
7. K. Shizu, H. Kaji, *Commun. Chem.*, **5**, 53 (2022).
8. X. Lv, J. Miao, M. Liu, et al., *Angew. Chem. Int. Ed.*, **61**, e202201588 (2022).
9. C.-Y. Chan, S. M. Suresh, Y.-T. Lee, et al., *Chem. Commun.*, **58**, 9377 (2022).
10. J. Gibson, A. P. Monkman, T. J. Penfold, *ChemPhysChem*, **17**, 2956 (2016).
11. T. J. Penfold, E. Gindensperger, C. Daniel, C. M. Marian, *Chem. Rev.*, **118**, 6975 (2018).
12. G. M. Sheldrick, *Acta Cryst. A* **71**, 3 (2015).
13. G. M. Sheldrick, *Acta Cryst. C* **71**, 3 (2015).
14. O. V. Dolomanov, L. J. Bourhis, R. J. Gildea, J. A. K. Howard, H. Puschmann, *J. Appl. Cryst.*, **42**, 339 (2009).
15. C. Bannwarth, S. Ehlert, S. Grimme, *J. Chem. Theory Comput.*, **15**, 1652 (2019).
16. F. Neese, *Wiley Interdiscip. Rev. Comput. Mol. Sci.*, **12**, e1606 (2022).

17. Y.-C. Cheng, X. Tang, R. Walia, et al., *Adv. Mater.*, **37**, 2500010 (2025).
18. J.-R. Wu, Y.-J. Yang, H.-T. Yuan, et al., *Chem. Sci.*, **17**, 5638 (2026).
19. T. Serevičius, R. Skaisgiris, G. Kreiza, et al., *J. Phys. Chem. A*, **125**, 1637 (2021).
20. G. Kreiza, D. Banevičius, J. Jovaišaitė, et al., *J. Mater. Chem. C*, **7**, 11522 (2019).

Giedrius Puidokas, Lukas Deltuvytis, Gediminas Kreiza, Kristupas Bagdonas, Karolis Kazlauskas

SIAURAJUOSČIŲ MĖLYNŲJŲ MR-TADF SPINDUOLIŲ KAMIENO IŠPLOKŠTĖJIMO SĄLYGOTAS UŽDELSTOSIOS FLUORESCENCIJOS SLOPINIMAS

S a n t r a u k a

Siaurajuosčiai mėlynieji multirezonansinės termiškai aktyvuojamos uždelstosios fluorescencijos (MR-TADF) spinduoliai yra perspektyvūs kuriant organinius šviestukus (OLED), pasižyminčius dideliu spalviniu sodriu. Vis dėlto, papildomos struktūrinės modifikacijos, padedančios išlaikyti spektrinį grynumą, gali turėti neigiamos įtakos uždelstajai fluorescencijai. Siekiant išsiaiškinti centrinio molekulinio kamieno planarizacijos įtaką mėlynajai emisijai ir tripletinių eksitonų panaudojimui, šiame darbe buvo tiriami du panašios struktūros tetraboro MR-TADF spinduoliai – **BO-4B** ir **c-BO-4B**. Nustatyta, kad praskiestuose tolueno tirpaluose abu junginiai pasižymi siaurajuoste fluorescencija giliai mėlynoje spektro srityje. **BO-4B** ir **c-BO-4B** emisijos maksimumai siekia atitinkamai 449 ir 444 nm, o juostų puspločiai – 14 ir 19 nm. Kvantinės chemijos skaičiavimai parodė, kad abu junginiai pasižymi panašaus tipo multirezonansinėmis S_1 būsenomis, tačiau išplokštėjusiam **c-BO-4B** yra būdingas didesnis energijų tarpas tarp singletinės ir tripletinės būsenų (ΔE_{ST}). Tą patvirtino ir žemoje temperatūroje 1 sv. % PMMA matricose išmatuoti fluorescencijos bei fosforescencijos spektrai. Kamieno planarizacija S_1 būsenos energijos beveik nepakeitė, tačiau sumažino T_1 lygmenį, todėl ΔE_{ST} išaugo nuo 95 iki 165 meV. Laikinės skyros fluorescencijos matavimai atskleidė, kad abiejų spinduolių sparčiosios fluorescencijos kvantinis našumas išliko vienodas (33 %), o uždelstosios fluorescencijos našumas drastiškai nukrito nuo 45 % iki 3 %. Remiantis supaprastintu kinetiniu modeliu, šis pokytis atitinka dviem eilėmis mažesnę atgalinės interkombinacinės konversijos (RISC) spartą. Taigi, gauti rezultatai rodo, kad kamieno planarizacija leidžia išsaugoti siaurajuostę sparčiąją emisiją, tačiau dėl nepageidaujamo T_1 būsenos energetinio poslinkio stipriai nuslopina uždelstąją fluorescenciją.